Icarus 205 (2010) 198–210

Contents lists available at ScienceDirect

Icarus

journal homepage: www.elsevier.com/locate/icarus

HiRISE images of yardangs and sinuous ridges in the lower member of the Medusae Fossae Formation, Mars

James R. Zimbelman [a,*], Lora J. Griffin [b]

[a] Center for Earth and Planetary Studies, National Air and Space Museum, MRC 315, Smithsonian Institution, Washington, DC 20013-7012, USA
[b] Geoscience Department, 4505 Maryland Parkway, University of Nevada, Las Vegas, NV 89154-4010, USA

ARTICLE INFO

Article history:
Received 18 October 2008
Revised 6 April 2009
Accepted 6 April 2009
Available online 7 May 2009

Keywords:
Geological processes
Mars, surface
Earth

ABSTRACT

HiRISE images of the lower member of the Medusae Fossae Formation (MFF) were used to identify characteristics of two specific landforms that are well expressed in this particular geologic unit; yardangs and sinuous ridges. Yardangs are wind-eroded ridges that are usually confined to arid environments where the bedrock materials can be easily eroded by windblown sand. Yardangs are common in the lower member of MFF, where many individual yardangs show evidence of a caprock unit overlying a more friable unit, most consistent with an ignimbrite origin for these MFF deposits. Heights of the yardangs in the lower member materials are generally less than a few tens of meters, in contrast to yardangs in the thicker middle member MFF materials to the east of the study area. The yardangs may form in materials comprised of discrete depositional units, and there is good evidence that at least a dozen such depositional events contributed to the emplacement of the lower member of MFF. The lower member yardang heights indicate aeolian erosion has removed at least 19,000 km^3 of lower member MFF materials. Sinuous ridges are elongate, positive-relief landforms that have been attributed to a variety of possible fluvial flow processes on Mars. Sinuous ridges are very common within exposures of the lower member of MFF. Multiple ridge types are present, but all forms seen at HiRISE scale are most consistent with some form of aqueous channel flow rather than other possible origins. The results from this initial examination of HiRISE images indicate the potential utility of comparing yardangs and sinuous ridges in the lower member to other members of MFF, although it remains to be determined if sinuous ridges are abundant in the younger MFF members.

Published by Elsevier Inc.

1. Introduction

Aeolian deflation and abrasion are common geomorphic expressions of erosion on rocky planets possessing atmospheres (e.g., Greeley and Iversen, 1985). Both erosive processes involve removal of loosely consolidated material by wind, resulting from the action of saltating sand. Eroded landforms are abundant in areas where there is or has been a large supply of sand, winds of sufficient speed and shear stress to transport the sand, and insufficient vegetation or large roughness elements to inhibit the full development of saltation. Aeolian erosion can both sculpt the bedrock being abraded, and also expose different components of the bedrock through differential erosion; this report will discuss both types of eroded landforms observed on Mars with the improved spatial resolution provided by images from the High Resolution Imaging Science Experiment (HiRISE) camera (McEwen et al., 2007a).

The study area is the western portion of the Medusae Fossae Formation (MFF), an enigmatic deposit present along nearly 100° of longitude over the martian equator (Fig. 1). The MFF deposits obtained their name during the global geologic mapping that utilized Viking Orbiter images for the mapping base, where the western portion of MFF was interpreted to be the oldest (lowest) member of the formation (Scott and Tanaka, 1986; Greeley and Guest, 1987). Considerable controversy has surrounded the possible formation mechanisms for MFF, as summarized below, but the hypothesis most consistent with both Viking and more recent mission data is some form of volcanic ash deposit, possibly emplaced as multiple ignimbrite events represented by alternating competent and more erodible layers (e.g., Scott and Tanaka, 1982; Bradley et al., 2002; Mandt et al., 2008). The attribute of the MFF materials most important to the present study is that they are very friable and easily eroded by the wind.

The HiRISE camera on the Mars Reconnaissance Orbiter (MRO) spacecraft is providing unprecedented views of the martian surface materials (e.g., McEwen et al., 2007b), including aeolian depositional and erosional features (Bridges et al., 2007). The HiRISE camera provides images with up to 25 cm/pixel spatial resolution (for

* Corresponding author. Fax: +1 202 786 2566.
E-mail addresses: zimbelmanj@si.edu (J.R. Zimbelman), lora.griffin@unlv.edu (L.J. Griffin).

0019-1035/$ - see front matter Published by Elsevier Inc.
doi:10.1016/j.icarus.2009.04.003

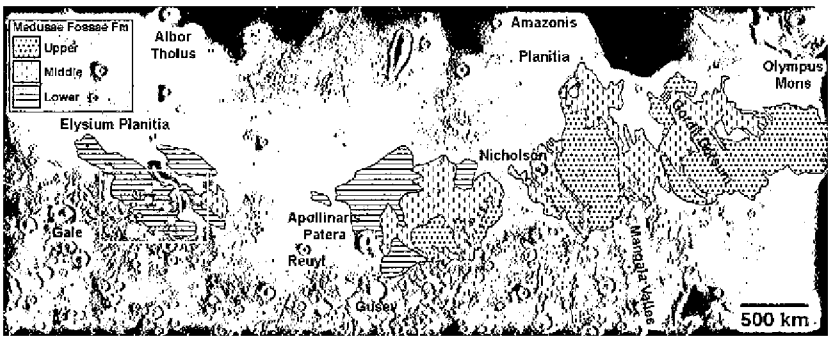

Fig. 1. Medusae Fossae Formation (MFF) units from 1:15 M geologic maps (Scott and Tanaka, 1986; Greeley and Guest, 1987) superposed on a shaded relief representation of MOLA topography (20°N to 20°S latitude, 130° to 230°E longitude). Selected prominent features are labeled; chart at upper left gives key to the MFF unit patterns. Outcrops of lower member materials are confined to the westernmost portions of MFF. White dots show locations of images in figures; white sinuous line shows location of long SR (see Fig. 13); white box indicates the study area.

map-projected products) with signal-to-noise that is substantially better than previous Mars imaging systems, including stereo for some retargeted locations, as well as color information, generally at a reduced resolution (McEwen et al., 2007a). HiRISE began its primary science phase in November of 2006, and since then thousands of high resolution images have been released to the scientific community, both through the HiRISE web site and through the Planetary Data System of NASA. The present report concentrates on yardang features eroded out of the western MFF deposits, and distinctive sinuous ridge features exposed by the removal of MFF materials in this region.

2. Background

2.1. Yardangs

A "yardang" is a wind-eroded ridge with a very streamlined shape (Ward and Greeley, 1984). Yardangs have been described as resembling an inverted ship's hull (Bosworth, 1922), although in many cases yardangs can be flat-topped. The windward face of the yardang is typically blunt-ended, steep and commonly the highest part of the feature, whereas the leeward end declines in elevation and tapers to a point; however, yardangs can take on a wide variety of forms (Whitney, 1983; Halimov and Fezer, 1989). West of the Rio Inca in Peru are streamlined yardangs up to 1 km in length, developed in clastic Tertiary sediments with elongate deflation pits, each rimmed by a resistant layer where wind abrasion locally penetrated the resistant layer and exposed more easily erodible rock at depth (McCauley et al., 1977). In the Lut Basin in southeastern Iran, yardangs up to 80 m high form very elongate ridges with flat to rounded summits, separated by troughs >100 m in width (McCauley et al., 1977); variations in the competency of the eroding bedrock, possibly related to variations in depositional conditions, may govern the resulting final shape of individual yardangs. Gypsiferous clay 10–15 cm thick blankets the Lut yardangs, which inhibits further growth of the water-carved gullies on the steep margins of the features (Walker, 1986).

Yardangs usually form parallel to one another, typically occurring as extensive fields. Yardang fields commonly occur as tight arrays, separated from one another by either U-shaped or flat-bottomed troughs, or as widely spaced, highly streamlined features on wind-beveled plains. Many yardang fields develop where strong unidirectional winds occur throughout much of the year (Hobbs, 1917; McCauley et al., 1977), but others, such as those in the Lut Desert, develop in regions of seasonally opposing winds. In areas of reversing winds, it appears that one wind direction is usually dominant, and the opposing wind is typically lighter and less frequent. Yardangs occupy only a small part of the Earth's surface, as they require conditions of great aridity, unidirectional or seasonally reversing winds, abundant sand, and a favorable bedrock material susceptible to aeolian erosion. McCauley et al. (1977) provide a global map of the major yardang localities around the world, also reproduced in Greeley and Iversen (1985, Fig. 4.23).

Interest in yardangs by the planetary community was fostered by the discovery of large yardang fields on Mars (McCauley, 1973; Ward, 1979) and by the widespread availability of aerial photography and satellite images for Earth (e.g., Mainguet, 1972; Ward, 1979; Halimov and Fezer, 1989). Malin et al. (1998) and Bridges et al. (2007) describe martian yardangs in MFF materials as seen in Mars Orbiter Camera Narrow Angle (MOC NA) images (with 6–1.5 m/pixel) and HiRISE images, respectively.

Wind tunnel experiments and selected wind measurements around mature yardangs suggest an ideal length-to-width ratio of 4:1 (Ward and Greeley, 1984), independent of scale. This value varies according to bedrock lithology, wind strength and direction, sand supply available to be mobilized by the wind, and the length of time the yardangs have been in existence. The ideal proportions are probably approached only after a long period of erosion. In Peru, well-developed streamlined yardangs have ratios ranging from 3:1 to 10:1 (McCauley et al., 1977). Dimensions can range from only a few meters to features with heights of as much as 200 m and several kilometers long (Mainguet, 1968). Knowledge of the wind flow around individual yardangs is based primarily on laboratory and theoretical determinations (Ward and Greeley, 1984; Whitney, 1985).

The significance of deflation in yardang evolution varies according to material induration (Whitney, 1985; Breed et al., 1989). In the sandstone yardangs of the Sahara there is little active removal of material from the ridge summits, as evidenced by a dark patina of varnish. Deflation (removal of silt- and clay-sized particles through suspension; Press and Siever, 1974, p. 333) appears to be a more important agent in yardangs found in less-indurated lacustrine material, such as siltstone yardangs 30–50 m high and up to 1.5 km long on the Pampa de la Averia, Peru, that possess smooth, streamlined shapes from base to crest (McCauley et al., 1977). The researchers cited above differ in their opinion as to the relative importance of abrasion and deflation in forming yardangs, and local conditions (in terms of wind intensity, sand availability, and the susceptibility of the bedrock to mechanical erosion) likely contribute to differing relative intensities of abrasion and deflation at various locations.

2.2. Sinuous ridges

The term "sinuous ridge" (SR) is used here to denote any elongate, positive-relief landform that is distinct from the usually shorter, straighter, mutually adjacent hills (inferred to be yardangs) that are visible throughout the MFF (Burr et al., 2009). Prior

workers have referred to similar landforms on Mars as 'raised curvilinear features' (RCFs) (e.g., Burr et al., 2006; Williams et al., 2007). The SRs show a wide variety of cross-sectional and planform shapes, network patterns, and landform associations. Sinuous ridges are exposed primarily (but not exclusively) on the westernmost exposures of the MFF, corresponding to the lower member of MFF (Burr et al., 2006, 2009). Nearly 200 SR sites covering areas ranging from tens to hundreds of square kilometers around the martian globe have been identified in m- to dm-scale images (Williams, 2007).

All published studies to date have interpreted SRs to involve a fluvial component in origin, but authors differ on the nature of the flow and the source of the water. Based on their curvilinear and bifurcating appearance, continuity relationships with valley networks and their similarity to terrestrial fluvial landforms, the SRs are interpreted to be the remnants of former fluvial channels formed by continually flowing water, with overprinting by branching channel networks, now expressed in inverted relief (Howard, 1981; Williams and Edgett, 2005; Burr et al., 2009). In addition to precipitation-fed surface runoff, other scenarios for generating fluids have been proposed in the formation of these landforms including impact-generated melt from ground-ice, glacial meltwater or subglacial streams (eskers) (Kargel and Strom, 1992; Nussbaumer, 2007; McMenamin and McGill, 2005; Burr et al., 2006).

Inversion of relief is a common attribute of landscape evolution and can occur wherever materials in valley bottoms are, or have become, more resistant to erosion than the surrounding materials (Pain and Oilier, 1995; Pain et al., 2007; Williams, 2008). Multiple processes can lead to the development of relief inversion including cementation of the valley floor (e.g., ferricrete, silicrete, calcrete, and gypcrete) (Mann and Horowitz, 1979), armoring of the valley floor by coarse grains, and infilling by a more resistant material (commonly a lava flow). Differential erosion removes the less resistant valley slopes and preserves the valley floor as a topographic high. Landscape inversion in either the upstream or downstream portion of a fluvial system can cause continuity of inverted relief with normal relief, but further study is needed to determine whether complete channel inversion is responsible for any of the exhumed ridges observed here (e.g., Pain and Oilier, 1995).

Howard (1981) hypothesized the existence of inverted fluvial channels in the Dorsa Argentia region of Mars, although he interpreted most of those ridges to be eskers. Subsequently, Williams and Edgett (2005) observed that some SRs have continuity relationships with traditional valley networks, evidence in support of a fluvial origin for those SRs. The preservation of fluvial networks on Mars is complex, with some channels that are filled and buried, others that have discontinuous preservation, and still others that are preserved in inverted relief (Williams and Edgett, 2005; Edgett, 2005). SRs interpreted to be inverted fluvial channels are present at various locations around the planet, including Arabia Terra, Lunae Planum, and within crater basins such as Eberswalde (Mangold et al., 2004; Malin and Edgett, 2003; Moore et al., 2003; Williams et al., 2005; Williams, 2007).

2.3. Medusae Fossae Formation

The Medusae Fossae Formation (MFF) comprises one of the most enigmatic deposits found on Mars. MFF materials are spread along the martian equator in the Amazonis and Elysium Planitiae regions (Fig. 1). On a global scale, MFF is divided into three subunits, all mapped as being Amazonian in age, the youngest era in the martian geologic record (Scott and Tanaka, 1986; Greeley and Guest, 1987), although some researchers think the MFF materials may include some Hesperian-age deposits (e.g., Schultz and Lutz, 1988; Schultz, 2007; Kerber and Head, 2009). Detailed mapping efforts to date have shown that the MFF materials are considerably more complex than was previously recognized (e.g., Zimbelman et al., 1997, 1999, 2000; Shockey and Zimbelman, 2005; Zimbelman, 2008). Nearly all of the MFF deposits occur within the boundaries of broad low thermal inertia (dust-blanketed) regions on Mars (Kieffer et al., 1977; Palluconi and Kieffer, 1981; Christensen, 1986), a situation that precludes easy remote sensing determination of the composition of the MFF materials. The western portions of MFF correspond to the least dust-covered sections of MFF, but dust will still complicate spectral measurements even here.

The MFF materials have generated many published hypotheses regarding their formation (summarized in Zimbelman, 1995; Zimbelman et al., 1997). The general similarity between terrestrial ignimbrites and MFF has been noted by several researchers (Malin, 1979; Scott and Tanaka, 1982, 1986; Chapman et al., 1989), and is currently considered to be the leading explanation for these deposits (Bradley et al., 2002; Mandt et al., 2008). Differential weathering within MFF materials, evident in imaging data available since Viking, has been interpreted to result from differing strengths between welded and non-welded zones in ignimbrites, by analogy with weathered ignimbrites (Scott and Tanaka, 1982; Mandt et al., 2008). Broad surface undulations in MFF were cited as evidence that MFF could be massive accumulations of variably indurated aeolian materials (Ward, 1979; Carr, 1981; Scott and Tanaka, 1986; Carr, 1996; Wells and Zimbelman, 1997). A variation on the aeolian theme is the interpretation that MFF, along with several additional eroded deposits around Mars, were emplaced as polar layered materials when the lithosphere of Mars wandered relative to the current pole positions (Schultz and Lutz, 1988), or resulted from deposition of massive volcanic ashfalls (Hynek et al., 2003). Some of the undulations on MFF are strikingly similar to broad folds in polar layered terrain, but in detail the MFF undulations differ significantly from polar deposit undulations (Bradley et al., 2002). The geophysical and geological demands of the polar wandering process remain difficult to reconcile with a long-lived Tharsis province and its influence on the rotation axis (Tanaka, 2000; Nimmo and Tanaka, 2005).

A structural approach was used to compare features observed along the Gordii Dorsum escarpment, and other linear valleys within MFF, to fractures associated with exhumed chemically altered materials that had been subjected to transcurrent faulting (Forsythe and Zimbelman, 1988; Forsythe et al., 1991). This hypothesis implies that the faults within MFF must be relatively old structures, now exposed by differential erosion of the altered materials. Unfortunately, subsequent remote sensing data have been unable to detect any evidence of chemical alteration within MFF while clearly documenting alteration products elsewhere on Mars (e.g., Bibring et al., 2006), due to the pervasive dust cover on the Tharsis region. A variation on the structural theme is that Gordii Dorsum is one of several transform faults associated with plate tectonic activity in the northern plains of Mars (Sleep, 1994). Subsequent mapping identified stratigraphic problems with the martian plate tectonic hypothesis (Pruis and Tanaka, 1995), but the structural features within and around MFF require additional study. The hypothesis that Mars had an ocean covering the northern plains (Parker et al., 1989; Baker et al., 1991) led to additional hypotheses for MFF, such as the interpretation that the deposits are eroded carbonate platform materials (Parker, 1991). The Thermal Emission Spectrometer has not detected any large exposures of carbonate rocks on Mars (Christensen et al., 2001; Glotch and Rogers, 2009), while the Compact Reconnaissance Imaging Spectrometer for Mars (CRISM; Murchie et al., 2007) instrument on MRO recently detected a rock layer of magnesium carbonate rocks in the Nili Fossae region of Mars (Ehlmann et al., 2008), well removed from the vicinity of MFF. Martian dust certainly complicates the remote determination of rock compositions on Mars, but it seems highly unlikely that CRISM would fail to detect any carbonates at

MFF (should it be comprised of large quantities of carbonate) while finding carbonate rocks elsewhere on the planet. Finally, MFF has also been suggested to be the result of rafted pumice accumulations along the southern margin of the hypothesized northern ocean (Mouginis-Mark, 1993).

The diversity of hypotheses of origin proposed for MFF indicate that these deposits have attracted considerable attention over the years, but thus far compelling evidence for their origin has proved elusive. Image interpretation of landforms on Mars has been augmented greatly by the quantitative topographic detail obtained from the Mars Orbiter Laser Altimeter (MOLA) (e.g., Smith et al., 1998; Sakimoto et al., 1999). The Mars Orbiter Camera (MOC) has returned many tens of thousands of high resolution images of Mars, including many detailed views of MFF (e.g., Malin et al., 1998; Malin and Edgett, 2001). The combination of MOC and MOLA data has provided important new constraints on MFF and its underlying terrains, as illustrated by evidence of dip on layers exposed within MFF (Sakimoto et al., 1999) and a detailed analysis of both imaging and topography that shows little similarity between MFF and the polar layered terrain (Bradley et al., 2002). Crater counts and superposition relationships among geologic units lead to an average age determination for the MFF as Amazonian (Tanaka, 1986; Werner, 2006), although earlier work suggests portions of MFF could date to the late Hesperian (Schultz and Lutz, 1988; Schultz, 2007; Kerber and Head, 2009). Recently the Mars Advanced Radar for Subsurface and Ionosphere Sounding (MARSIS) on the Mars Express spacecraft revealed that the eastern portions of MFF are up to 2.5 km in thickness, with all MFF deposits laying unconformably on the underlying northern plains materials; dielectric properties in MFF are consistent with either dry or ice-rich conditions inside the deposits (Watters et al., 2007). The Shallow Radar (SHARAD) on the MRO spacecraft similarly revealed that the MFF sediments are superposed on the northern plains materials, with virtually no evidence of internal reflectors, and there is no compelling evidence for ice preserved within the MFF materials probed to date (Carter et al., 2009).

3. Methodology

HiRISE images (as of July 2008) that included exposures of the lower member of MFF within the MC 23-NW quadrangle (0° to 15°S latitude, 135° to 157.5°E longitude) were examined for this study. As an integral component of a NASA-funded project to produce a new geologic map of the MC 23-NW quadrangle, the current investigation focused on the portion of this quadrangle where global geologic mapping (Greeley and Guest, 1987) identified exposures of the lower member of MFF (0° to 8°S latitude, 142° to 155°E longitude; see white box in Fig. 1). Thirty-five HiRISE images were inspected within this study area, where several distinctive attributes of both yardang and sinuous ridge features were consistently observed on the MFF materials. Also examined were two coincident HiRISE images (PSP_003398_1910 and PSP_003543_1910, which comprise a stereo pair) of a location at the northern margin of an exposure of the middle member of MFF, and one HiRISE image of the layered deposit that mantles the central peak of Gale crater (PSP_008938_1910). Features at these two locations were compared with those that are common on lower member MFF exposures. Table 1 lists the HiRISE images referenced in this report, which are illustrative of the major characteristics observed in all HiRISE images examined in detail for this study. Table 1 is by no means a comprehensive list of HiRISE images in the area, but these images are most instructive for examining both yardangs and sinuous ridges in the study area. North is to the top in all HiRISE subscenes shown here, and all image centers are listed in aerocentric coordinates. No comprehensive measurement campaign was undertaken involving all of the released HiRISE images within the study area; however, measurements were made of selected features, as described below.

4. Results

4.1. Yardangs

Yardangs are well expressed in the lowest member of MFF, perhaps related to the inference that the lowest member appears to be the most severely eroded of the three MFF members (Scott and Tanaka, 1986; Greeley and Guest, 1987). The yardangs in the lower member of MFF display a variety of shapes and planforms, but most are represented by the yardangs visible in image PSP_000828_1805 (Fig. 2). The yardang has an elongate (oval) plan form, commonly with a resistant caprock component that is closer to the inferred upwind side of the feature than to the opposite end. The presence of a resistant caprock within MFF materials was previously observed in Viking (Scott and Tanaka, 1982) and MOC (Malin et al., 1998; Malin and Edgett, 2001; Mandt et al., 2008) images, cited as one of the primary observations supporting an ignimbrite origin for the MFF materials (Scott and Tanaka, 1982; Mandt et al., 2008). HiRISE images now reveal how the caprock erodes into discrete boulders (up to 5 m across) that remain coherent after falling from the caprock margin (e.g., Fig. 2), providing clear evidence of the competency of resistant-layer sediments within the lower MFF materials.

Length:width ratios of yardangs in MFF materials range from ~2:1 (e.g., Fig. 2) to >10:1 (Ward, 1979), with the majority approaching a 4:1 ratio (e.g., Fig. 3) that is representative of the minimum drag configuration (Ward and Greeley, 1984). Shadow lengths indicate yardang heights typically were a few tens of meters (e.g., 35 m height for the yardang shown in Fig. 2), with the highest features usually those still possessing a resistant caprock unit (e.g., Fig. 2). Flank textures on yardangs in lower member MFF materials are generally bland even in the HiRISE images. Rarely, some internal layering within the more easily eroded portions of the yardang can be inferred from lineations of resistant knobs present within the flank materials (image PSP_003690_1755, Fig. 3), but most flanks show no coherent patterns or textures at HiRISE resolution. Even when a coherent caprock unit is not evident at the summit of yardangs, m-scale blocks are usually abundant on or around the yardang flanks (Fig. 4a), providing strong evidence that a caprock unit was present there in the past.

4.1.1. Layering

The yardangs are present in MFF materials that are layered at a scale broader than the size of an individual yardang; such layering often is better expressed in a Context Imager (CTX; Malin et al., 2007) scene at 5.3 m/pixel than in a HiRISE image (see CTX inset in Fig. 3). This large-scale layering is evident in images even where individual yardangs are not resolved, such as frame I7557001 from the Thermal Emission Imaging System (THEMIS; Christensen et al., 2004), which shows the broad layering around the Fig. 3 site in a daytime thermal infrared image at 100 m/pixel.

Within an individual HiRISE frame, occasionally yardangs with different orientations are present on different local layers within the MFF materials. For example, image PSP_001448_1735 shows fields of individual yardangs with an inferred wind from the WNW (e.g., Fig. 4a), yet other poorly developed yardangs with an E–W orientation are eroded into a separate (stratigraphically higher) layer of MFF material near the top of the same image (Fig. 4b). This observation is consistent with multiple yardang directions recorded on the surfaces of different layers within the upper member of MFF as observed in Viking images, inferred to indicate that multiple paleowind regimes may be preserved at some locations (Wells and Zimbelman, 1997).

Table 1
Information for HiRISE images used in figures.

Frame Number	Latitude[a]	Longitude[a] (E)	Resol.[b] (cm/p)	Solar Inc.[c] (deg)
TRA_000828_1805	0.5 N	142.1	25	35
PSP_001448_1735	6.3 S	149.3	25	32
PSP_002002_1735	6.2 S	151.4	25	33
PSP_002279_1735	6.2 S	151.4	25	31
PSP_003398_1910	11.0 N	198.0	25	30
PSP_003543_1910	11.0 N	198.0	25	31
PSP_003690_1755	4.5 S	147.3	50	38
PSP_006683_1740	6.0 S	153.6	25	50
PSP_006815_1780	2.1 S	148.8	50	50
PSP_007382_1770	3.1 S	146.4	25	45
PSP_007395_1775	2.5 S	151.1	25	45
PSP_007975_1755	4.7 S	154.9	50	38
PSP_008938_1750	4.9 S	138.4	25	32

[a] Latitude and longitude are for the image center, and are for an aerocentric coordinate system.
[b] Map-projected image resolution.
[c] Angle of solar incidence above the horizon.

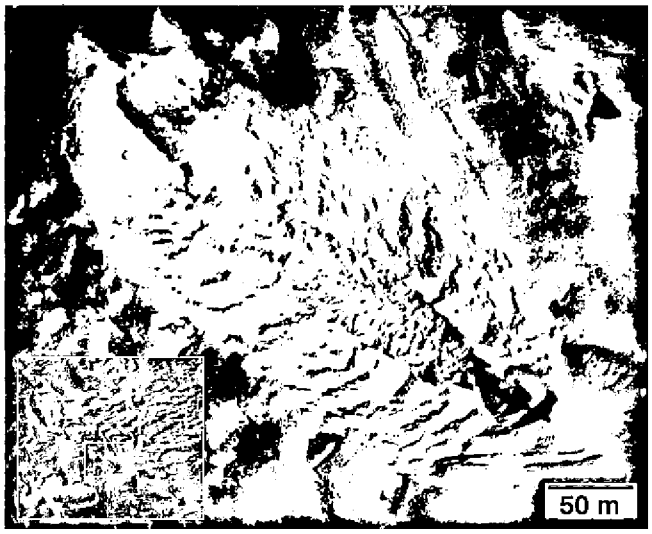

Fig. 2. Yardang in lower member of MFF. Caprock unit is the source of boulders on lower flanks of the yardang. The caprock is closer to the feature edge at the lower right than at upper left, suggesting the predominant eroding wind was from the ESE. North is at the top in all HiRISE subscenes shown here. TRA_000828_1805, 0.5°N, 142.1°E. Inset: location within portion of browse image.

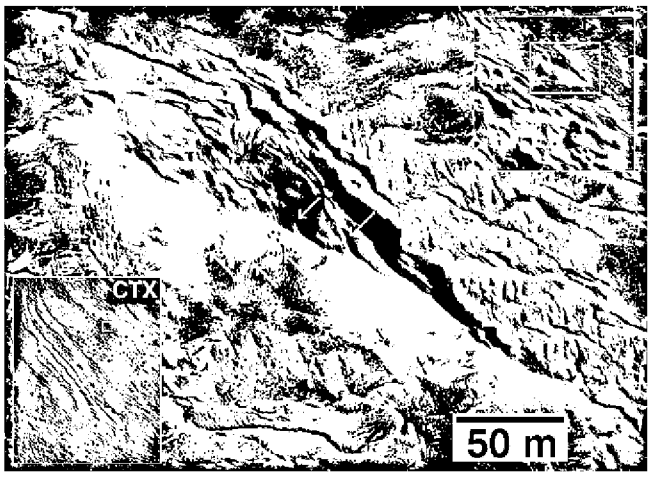

Fig. 3. Yardang in lower member of MFF. Probable internal layering is visible at some locations on the flanks of the yardang (arrows). No caprock is present, nor are boulders observed here. Thickest portion of yardang is at upper left end, suggesting the predominant eroding wind was from the WNW. PSP_003690_1755, 4.5°S, 147.3°E. Inset, upper right: location within portion of browse image. Inset, lower left: Portion of CTX frame P02_003690_1756, 5.3 m/pixel, indicating location of browse image subscene and broad layers.

Portions of the lower member MFF materials display repeated sequences of prominent cliff-forming (resistant) layers separated by more easily eroded material consisting of relatively shallow slopes (image PSP_006815_1780, Fig. 5), suggestive of a cyclic deposition for the whole package of MFF materials at some locations. HiRISE image PSP_008938_1750 shows that thick deposits on the interior of Gale crater, well to the west of the current mapped boundary of MFF (Fig. 1), display a similar sequence of alternating cliff-forming and more friable layers, including the presence of many blocks likely derived from the cliff-forming layers (Fig. 6).

4.1.2. Uneroded MFF surface

The appearance of the upper surface of MFF materials is instructive when considering the mode of emplacement of MFF deposits (image PSP_007382_1770, Fig. 7a). The uneroded upper surface of the lower member MFF materials gives the appearance of a surface that has been heavily mantled, resulting in greatly subdued rims of two impact craters visible through the mantle (the subdued craters both are >100 m in diameter); this mantling material could easily have totally obscured all smaller craters. The thickness of the MFF material deposited on the buried craters is likely >10 m (in order to produce the subdued appearance of both large crater rims) but <50 m (in order to not completely obscure the smaller 110-m diameter crater). Since the emplacement of the MFF mantling deposit, numerous relatively fresh (sharp-rimmed) impact craters (all <20 m in diameter) have impacted onto the surface of the MFF materials, possibly including many secondary craters. In general, ejecta deposits from the superposed fresh craters are not clearly evident, even at HiRISE resolution, so that some deposition likely post-dated even the fresh craters. Yardangs and other scour features are evident near the bottom of the same HiRISE frame showing the MFF upper surface (Fig. 7b), demonstrating that removal of the MFF mantle can result in yardang landforms.

4.1.3. Comparison with a yardang in eastern MFF

The yardangs in the lower member MFF materials are eroded from sediments generally tens of meters in thickness. This situation can be contrasted to a yardang from the middle member of MFF, which formed from a deposit of substantial thickness (Fig. 8a). This middle member yardang is significantly larger than

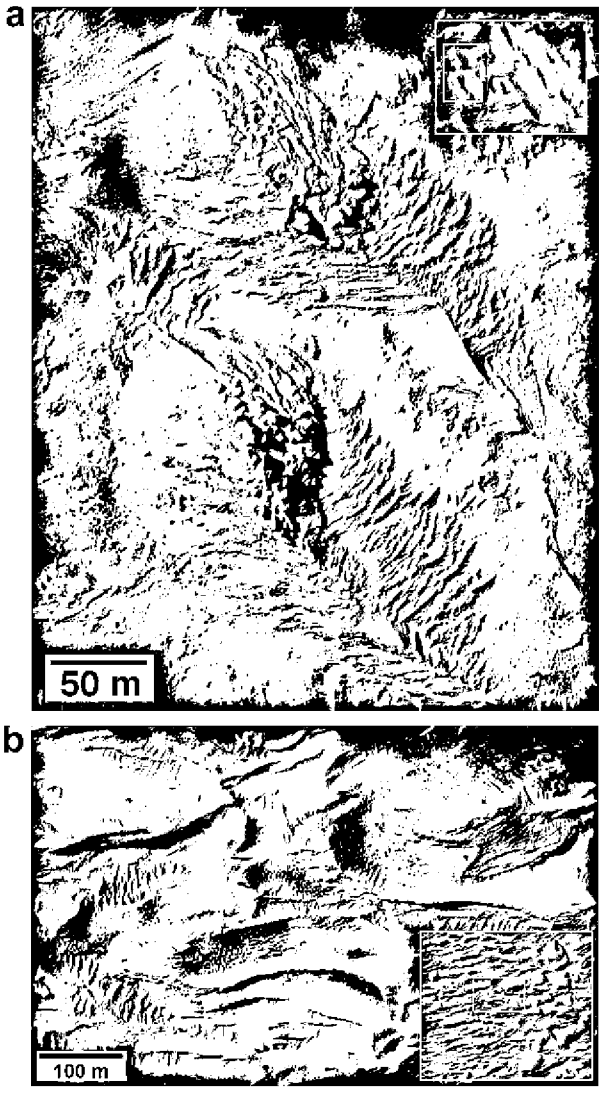

Fig. 4. Yardangs in lower member of MFF. (a) Blocks on flanks suggest a caprock unit, like that in Fig. 2, was originally present. Thickest portions of both yardangs occur on the upper left side of both features, suggesting that the predominant eroding wind was from the WNW. (b) Yardangs in upper part of same image as (a). Scouring and blunt ends of developing yardangs indicate the predominant eroding wind was from the W. Both views, PSP_001448_1735, 6.3°S, 149.3°E. Inset: location within portion of browse image.

any yardang observed on the lower member of MFF, in terms of both planform dimension and thickness. The length of the middle member yardang is several times that of the largest individual yardangs observed in the lower member of MFF. Also, the planar top (see inset in Fig. 8a) of the middle member yardang is quite distinct from the rounded shape of most of the lower member yardangs (Figs. 2–4). The strong shadow cast by the eastern edge of the middle member yardang provides excellent shadow lengths, indicating that this one yardang ranges from 65 to 105 m in thickness, which is more than twice the height of the largest lower member yardangs. Oblique illumination of the southern tip of the middle member yardang highlights very subtle relief (Fig. 8a); importantly, no cliff-forming (resistant) layers are evident anywhere throughout the entire thickness of the yardang, although subtle scalloping on the yardang face suggests the presence of internal layering on the scale of a few meters. Such m-scale internal layering is even more evident along the eroded edge of the middle member MFF deposit inside a crater located very close to

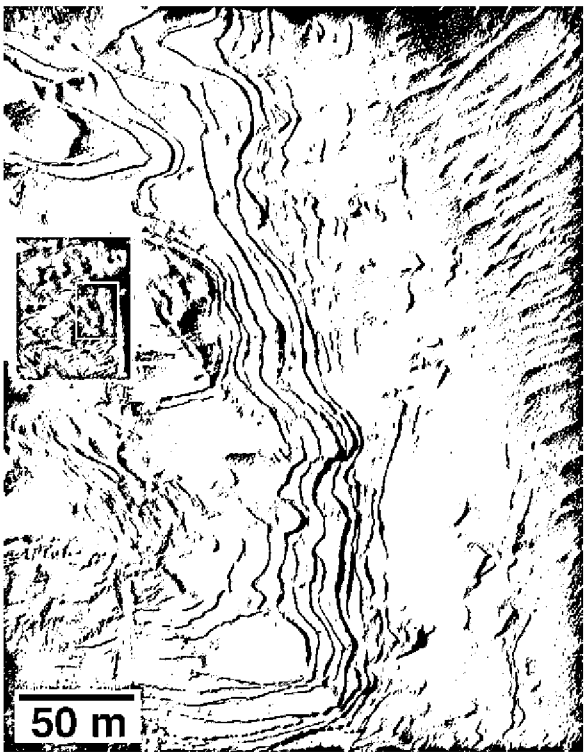

Fig. 5. Layering within lower member of MFF. Sequence of >10 cycles of alternating resistant (cliff-forming) and friable (slope-forming) layers. PSP_006815_1780, 2.1°S, 148.8°E. Inset: location within portion of browse image.

Fig. 6. Blocks weathering from resistant (cliff-forming) layers within deposits in Gale Crater. Layering is potentially analogous to layers visible in Figs. 3 and 5, suggesting it may be an outlier of lower member MFF materials. PSP_008938_1750, 4.9°S, 138.4°E. Inset: location within portion of browse image.

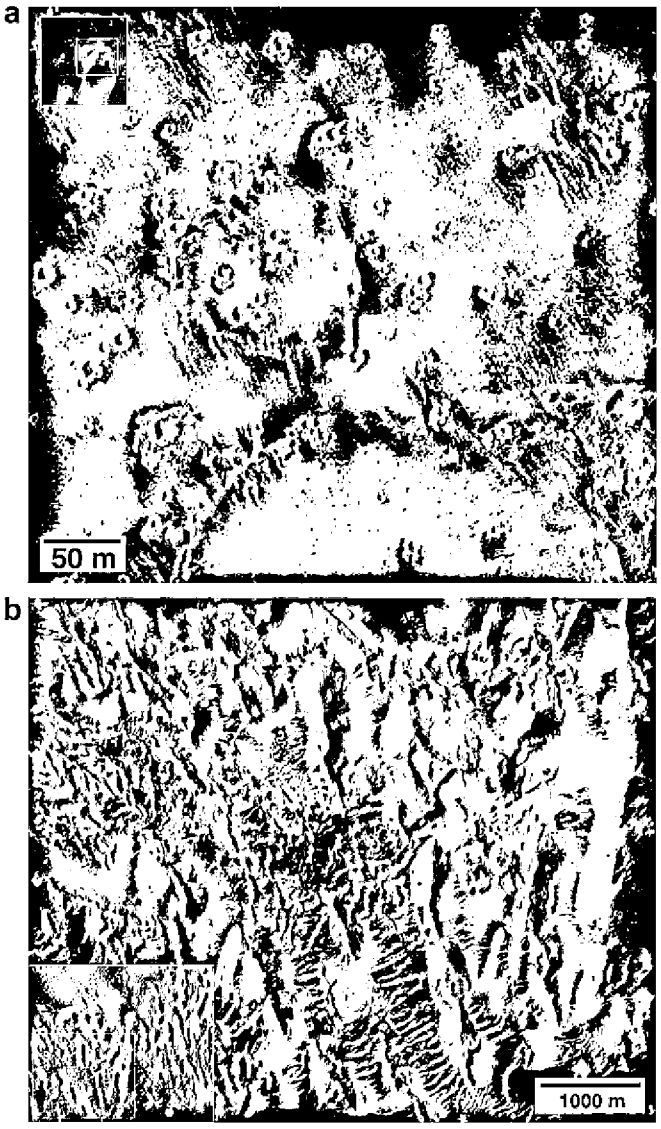

Fig. 7. (a) Mantled upper surface of lower member of MFF. Very subdued appearance of two craters >100 m in diameter. Fresh-rimmed craters <20 m in diameter generally lack visible ejecta. Inset: location within portion of browse image. (b) Yardangs present near the bottom of the same image shown in (a), eroded within the same MFF materials. Portion of browse image (inset gives context in browse image). Both views, PSP_007382_1770, 3.1°S, 146.4°E.

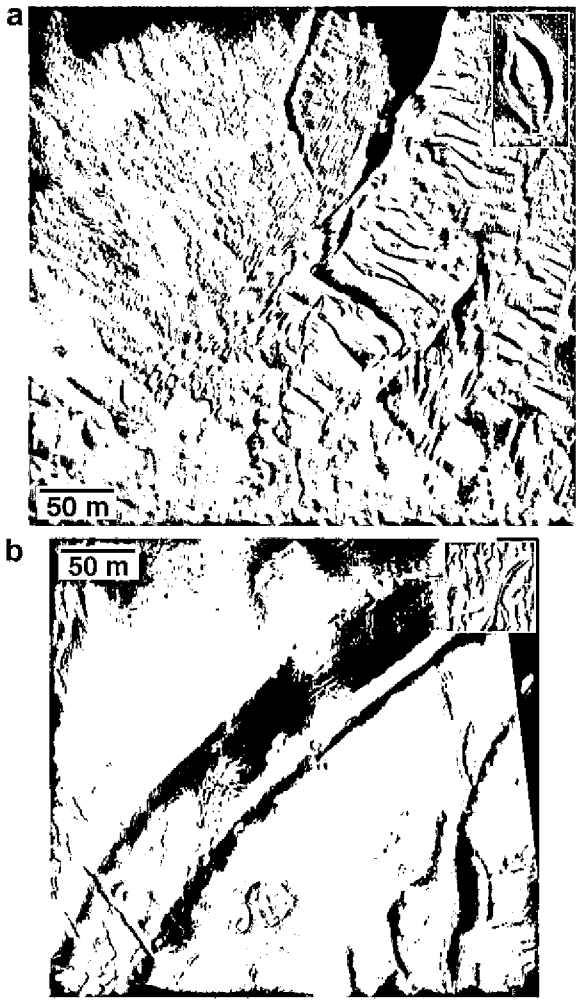

Fig. 8. (a) Anaglyph showing relief along the southern tip of a yardang from the middle member of MFF. Red (left): PSP_003398_1910, 11.0°N, 198.0°E. Blue and green (right): PSP_003543_1910. Inset: location of anaglyph in portion of browse image. (b) Anaglyph showing flat crest, steep margins, and ridges exposed by erosion of a sinuous ridge. Red (left): PSP_002279_1735, 6.2°S, 151.4°E. Blue and green (right): PSP_002002_1735. Inset: location of anaglyph in portion of browse image. Both anaglyphs were produced from map-projected HiRISE products, which removes regional-scale topography as documented by MOLA.

the middle member yardang in Fig. 8a (Fig. 9). Comparable evidence of such uniform m-scale layering within the lower member MFF materials is lacking to date.

The southern end of the middle member yardang is faceted when viewed in stereo (Fig. 8a); that is, the erosion has produced discrete faces that extend over lengths of many tens of meters. These facets are comparable to features observed on ventifacts (wind-eroded rocks and boulders; Bridges et al., 1999, 2005), although at a scale perhaps two orders of magnitude larger than that normally encountered in ventifacts. No blocks are visible at the base of the middle member yardang (Fig. 8a), in contrast to the blocks common on and around most of the lower member yardangs (Figs. 2–4). The differences between the middle member yardang example and the majority of the lower member yardangs illustrate how the deposition, erosion, and preservation of internal layering varied between the emplacement of the lower and middle member materials.

4.2. Sinuous ridges (SRs)

SRs are abundant in the lower member of MFF (unit Aml from Scott and Tanaka, 1986; Greeley and Guest, 1987), and they are mostly concentrated within, or proximal to, a broad depression that is present between two lobes of Aml materials within the study area. Six types of SRs were observed during this study, including flat-crested, narrow-crested, round-crested, branching, non-branching, and multilevel features; these designations have been adapted from the classification scheme described in Burr et al. (2009), which was derived from the study of THEMIS and MOC images. Two or more of these different types may be used to describe individual SRs or SR groups. For example, flat-crested SRs commonly occur as multilevel branching features.

4.2.1. Flat-crested

Many SR features display broad, typically planar crests, generally tens of meters across, that terminate at sharp edges and near-vertical high-angle slopes (Figs. 8b, 10, and 11). Shadow

Fig. 9. Layering exposed on eroded middle member MFF materials within a crater adjacent to the yardang in Fig. 8a. PSP_003398_1910, 11.0°N, 198.0°E. Inset: location within portion of browse image.

length sampling along several individual ridges indicates that flat SR thicknesses range from <1 m to >10 m. Induration and erosion that occurred throughout the history of the channel and the surrounding sediments strongly influenced the SR thickness variations observed in HiRISE images, but the present eroded state of the features provides at best a rough estimate of the apparent thickness of the original channel deposits. Crests are described as flat because they exhibit little change in elevation across their breadth and contain no visible medial ridge (Fig. 8b). SRs with flat crests occur most commonly as branching, multilevel features, but rare occurrences of flat-crested ridges with shapes similar to terrestrial migrating streams are also present. The occurrence of flat-crested SRs displaying wispy parallel ridges similar to point bar migration in meandering streams is less common, but is prominent in images PSP_008621_1750 and PSP_007975_1755 (Fig. 12a), and meander morphology is spectacularly displayed for SRs in image PSP_006683_1740 (Fig. 12b). Flat-crested SRs are primarily located along the margins of a broad depression between the two lobes of lower member materials in the western portion of the MFF (left side of Fig. 1). Terrestrial sinuous ridges near Green River, Utah, described in previous work, provide compelling evidence for the existence of inverted paleochannels with flat crests that are analogs to the SR features on Mars (Williams, 2008; Williams et al., 2009).

4.2.2. Narrow-crested

These SRs are also commonly flat-crested, but they usually display a prominent medial crest <10 m wide, with slopes extending directly from the edges of the medial ridge to the base. The ridge base is typically at least three times as wide as that of the crest, perhaps related either to mass-wasting or to aeolian deposition along the margins of the ridge. Preliminary shadow length measurements for several ridges indicate an estimated average height of <10 m. The narrow-crested SRs are most commonly expressed as individual ridges with high sinuosity located in areas of lower elevation. Narrow-crested SRs typically are expressed as individual, non-branching features with mature sinuosity, rarely occurring as branching or multilevel deposits. Flat-crested and narrow-crested SR classifications both are subsets adapted from the "Thin" type described in Burr et al. (2009).

4.2.3. Round-crested

Round-crested SRs display a convex-up shape when viewed in vertical cross-section perpendicular to length, with rounded, gently sloping edges. HiRISE image PSP_007395_1775 displays a segment of the most prominent expression of round-crested SR morphology within the lower member of MFF (Fig. 13). The image contains a segment of a rounded ridge with well-developed sinuosity that, when correlated with CTX and MOLA data, extends >200 km down the middle of a low-elevation basin present between two lobes of the lower member MFF within the study area (see line in Fig. 1; Griffin and Zimbelman, 2009). Thickness varies more widely along this long single ridge than for flat-crested ridges in general, but averages slightly over 5 m high; this extensive SR is about 32 m wide and varies only slightly along its entire length.

4.2.4. Branching

Branching SRs observed in the study area are characterized by the occurrence of interconnecting raised ridges. The branching ridges are expressed as both fan-like structures and with planforms similar to that of terrestrial braided or anastomosing streams (Figs. 10 and 11). Branching SRs typically include flat-crested SRs of varying size that are most commonly located on the margins of the broad basin between the two lobes of lower member MFF materials in the study area. Crest widths of branching SRs measured here range from 10 to 60 m, with overall ridge thickness (height) obtained from shadow lengths that ranges from 0.8 to 11.0 m. An increase in the number of branches with decreasing elevation is a common attribute of branching SRs, but additional examples should be studied to evaluate this trend. Branching configurations similar to the planform of terrestrial braided streams are exposed within a lower layer of the small fan in image PSP_007975_1755 (Fig. 10), but this morphology is not common throughout the lower member of MFF within the study area.

4.2.5. Non-branching

SRs that are isolated along their length, with no interconnecting branches, are termed here as non-branching. These SRs are most commonly expressed as elongate, moderately sinuous to highly sinuous features, and they are usually located proximal to large, well-developed yardang fields (Fig. 13). Non-branching SRs occur as round-, flat-, and narrow-crested sinuous ridges.

4.2.6. Multilevel

Some SRs consist of raised fan-shaped landforms that are superposed successively above one another (Figs. 10 and 11). The multilevel SRs occur on the easternmost margin of the depression between the two lobes of lower member MFF materials; none were observed on more topographically level terrains. Most multilevel SRs contain successive layers of flat-crested SRs occurring sub-parallel to one another, suggesting multiple events all with a similar emplacement direction.

4.2.7. Additional observations

Flat-crested SRs are overlain in many locations by a thick layer of competent MFF material (Fig. 14). The superposition of this thick

Fig. 10. Sinuous ridges (SRs) with braided or anastomosing pattern exposed within a small branching SR fan. The branching SRs are generally multileveled and distributary in nature, with the abundance of SR reaches increasing with decreasing elevation. PSP_007975_1755, 4.7°S, 154.9°E. Inset: location within portion of browse image.

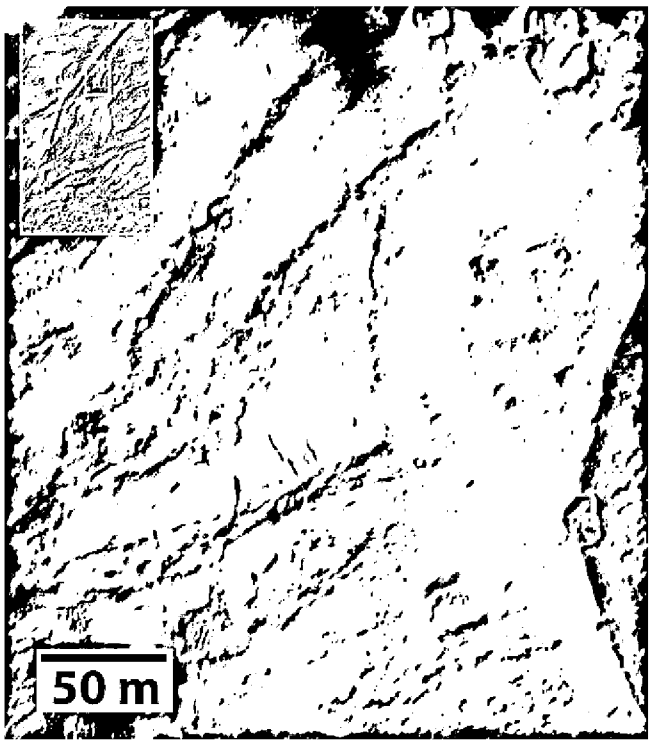

Fig. 11. Flat-crested SRs superposed on older SRs within the lower member of MFF indicate that multiple aqueous events may have occurred contemporaneously with the deposition of lower member MFF materials. PSP_007975_1755, 4.7°S, 154.9°E. Inset: location within portion of browse image.

unit above SRs in the lower member MFF may include isolated portions of the middle member of MFF, but no definitive small-scale outliers of middle member MFF materials have been identified to date within the study area. Shadow lengths of the mantling component (overlying all SR types described above) indicate thickness ranges from 8 to 60 m for the images within the study area; this mantling material is intensely eroded, locally displaying small (<10 m) faceted surfaces comparable to facets scoured on the middle member MFF yardang discussed above (Fig. 8a).

A rather unique surface is shown in Fig. 15, where a flat-crested SR is superposed on two stratigraphic layers that comprise a thin deposit with a very distinctive erosional texture. This 'etched' layer has an irregular texture at a scale <10 m, comprised of peaks and swales that indicate intense erosional scour occurred here. This distinct layer is exposed at multiple locations between SRs throughout the small fan in image PSP_7975_1755 (see inset of Fig. 10). The consistent position of this etched layer beneath the SRs indicates that it was deposited prior to the emplacement of the SRs. Further examination of this unique layer outside of the study area may reveal clues to the paleoenvironment immediately preceding the formation of SRs, which itself appears to have oc-

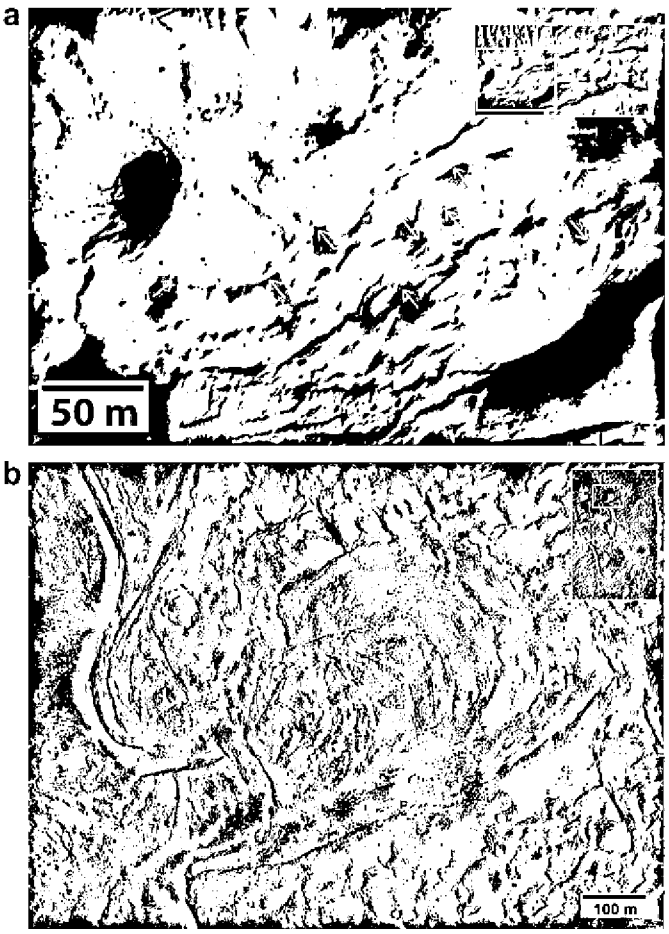

Fig. 12. Meanders of SRs. (a) Wispy meandering ridges (arrows) occurring at a topographic low point along the southern edge of a broad basin between two lobes of the lower member MFF materials demonstrates multiple shifts in deposition analogous to migrating point bars. PSP_007975_1755, 4.7°S, 154.9°E. Inset: location within portion of browse image. (b) Well-developed cut-off meanders. A cut-off meander coupled with migrating crescentic ridges is analogous to oxbow lake morphology commonly present on terrestrial flood plains. The presence of such mature meanders within the lower member MFF materials strongly suggests a persistent channelized fluvial environment existed during its formation. PSP_006683_1740, 6.0°S, 153.6°E. Inset: location within portion of browse image.

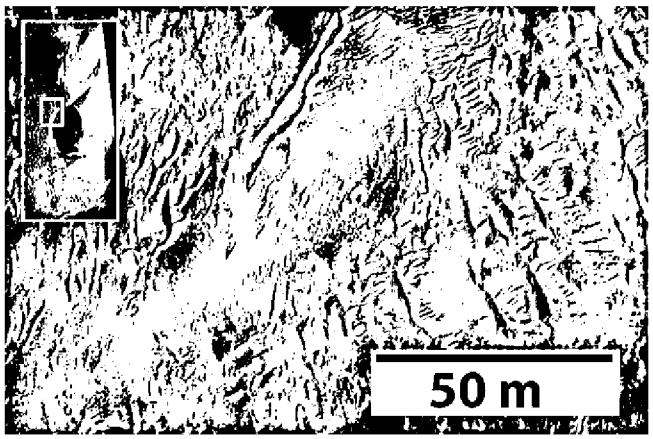

Fig. 13. Portion of an isolated SR that follows the low point of a broad basin between two lobes of lower member MFF materials in the study area (see white line in Fig. 1). This single SR extends for hundreds of kilometers, with an average height and width of 5 m and 32 m, respectively. PSP_007395_1775, 2.5°S, 151.1°E. Inset: location within portion of browse image.

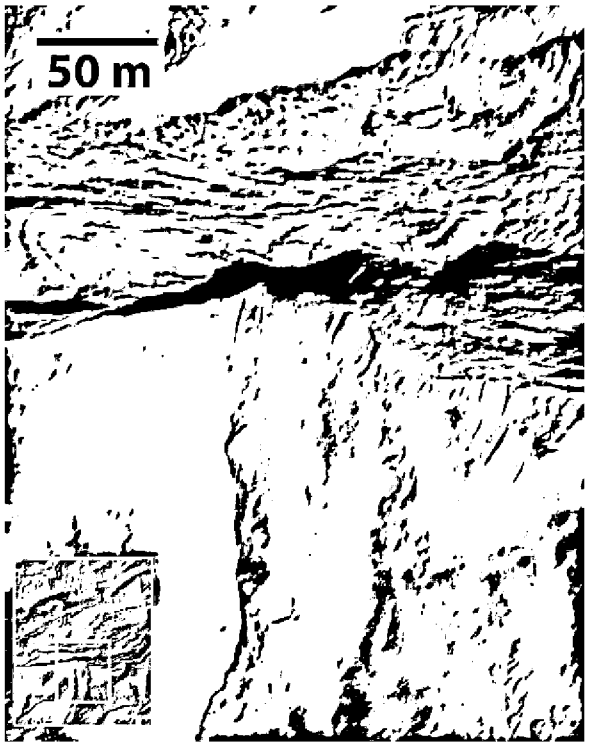

Fig. 14. Scoured lower member MFF materials superposed on a flat-crested SR at the base of a small fan on the eastern margin of a broad basin between two lobes of the lower member MFF materials in the study area. PSP_007975_1755, 4.7°S, 154.9°E. Inset: location within portion of browse image.

curred preferentially during an early stage of the overall emplacement of MFF materials (Burr et al., 2009).

5. Discussion

5.1. Origin of the lower member of MFF

The observations reported here have some important implications for the proposed origins for the lower member of MFF. The common occurrence of alternating resistant (cliff-forming) and friable (slope-forming) components of the lower member MFF materials (e.g., Fig. 5) is difficult to reconcile with an aeolian (loess-like)

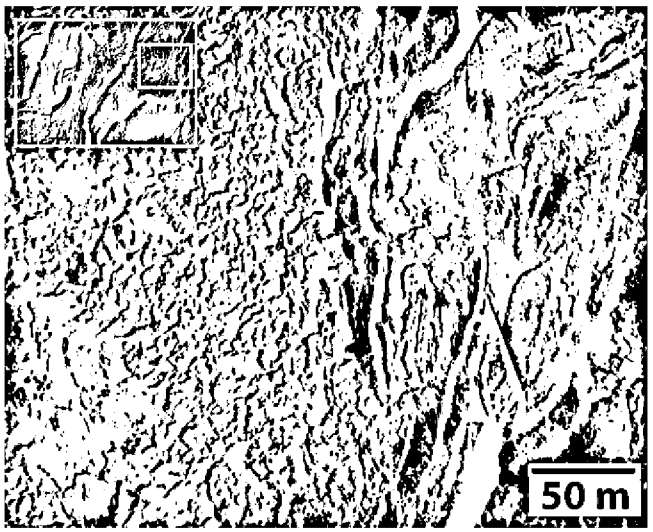

Fig. 15. SRs exposed within a small branching fan are underlain by a highly textured layer (left side of image) of material that may provide clues to the paleoenvironment that preceded SR emplacement within lower member MFF materials. PSP_007975_1755, 4.7°S, 154.9°E. Inset: location within portion of browse image.

depositional emplacement without cyclic variations in the climate that periodically induced enhanced induration of some of the materials. Little evidence of systematic changes in the direction of the eroding wind was noted during our examination of the HiRISE images in the study area (with the exception of Fig. 4, as discussed above), something that might be more widespread through the region if cyclic regional climatic changes were the cause of the layered sequences evident throughout the lower member MFF deposits. Instead, we interpret the limited exposures of multiple wind directions by yardangs in lower member MFF materials to be more indicative of the limited potential for preservation and exhumation of multiple trends. The alternation of resistant and friable layers is quite consistent with an ignimbrite emplacement, potentially involving dozens of discrete eruption events to contribute to the formation of the multiple layers observed in the lower member of MFF.

Large-scale layering (inset of Fig. 3) may represent multiple depositional events, as discussed above, while an individual yardang (Figs. 2–4) is more likely to represent only a portion of one such depositional event. Lower member MFF deposits outcrop over an area of ~550,000 km^2 (Fig. 1; Scott and Tanaka, 1986; Greeley and Guest, 1987), so that the height of the yardangs in the lower member (use 35 m, from Fig. 2) implies that a lower limit of ~19,000 km^3 of lower member MFF materials must have been removed by aeolian erosion to produce the observed yardang fields. The volume of material removed would be significantly larger if the yardangs do not represent the full deposit thickness, which seems quite possible. The layered characteristics of the Gale crater deposits (Fig. 6), similar to multiple layers exposed within MFF (Fig. 5), lead us to hypothesize that the Gale materials are actually outliers of a previously much more extensive lower member MFF deposit, consistent with recent mapping that has identified outliers of layered materials between Gale and the globally mapped boundary of MFF (Zimbelman, 2008).

In instances where images reveal distinct vertical segregations within MFF materials (e.g., Wells and Zimbelman, 1997), the inferred vertical variation typically cannot be traced much beyond the extent of a single image, whether HiRISE, MOC, or THEMIS images. This observation indicates that MFF materials can be locally homogeneous at the 10-m scale across length scales on the

order of a kilometer, but not on the order of 100 km. The length scale of homogeneity within MFF materials places an important constraint on some of the proposed hypotheses of origin for these enigmatic deposits. Deposition that is homogeneous at length scales of a kilometer but heterogeneous at length scales of 100 km would not appear to be consistent with the very regular layering evident in polar deposits, where some discrete layers can be traced over hundreds of kilometers at MOC resolution (Byrne and Murray, 2002; Edgett et al., 2003; Fishbaugh and Head, 2005). However, ignimbrite emplacement could be consistent with the homogeneity arguments just described, particularly if multiple vent locations are invoked, which is consistent with the ignimbrite origin for MFF derived from the most recent survey of MFF at MOC resolution (Mandt et al., 2008).

5.2. Origin of sinuous ridges (SRs)

The characteristics of sinuous ridges viewed at HiRISE resolution appear to be much more consistent with a paleochannel environment than with an esker type of emplacement. SRs examined in this study also demonstrated a relationship between regional topography and SR morphology. Flat-crested multilevel branching SRs were observed generally to be located along the inner perimeter of the broad shallow basin between the two lobes of the lower member MFF exposed within the study area. Narrow-crested and round-crested non-branching SRs are found primarily in areas where topographical changes are minimal over the length of the SR. The maturity of sinuosity expressed by some SRs (Fig. 12b) demonstrates further the likelihood of long-term aqueous flow, both for generation of the meanders themselves and for associated oxbow features that are most easily interpreted to be cut-off meanders of former river channels.

The variability of SR morphologies requiring diverse water flow regimes suggests that different areas may have experienced several types of aqueous events. The multilevel stratigraphy, braided patterns, and the distributary nature of branching SR reaches are difficult to explain without the presence of aqueous water. Episodic aqueous events such as flooding or precipitation are needed to facilitate the development of these types of networks. Unlike the stacked multilevel SRs, extended periods of aqueous water flow are essential in the formation of the mature sinuosity displayed in some meandering ridges. Some bifurcated ridge bends display what we interpret to be cut-banks and subsequent migrating point bars at precisely the places where such features would be found in a fluvial system (e.g., Fig. 12a). Migrating meanders suggest long-term fluvial processes, supported by the presence of very mature sinuosity in SRs that form multiple cut-off meanders and oxbow-like features (Fig. 12b). This same type of long-term water regime is also necessary to explain the presence of thin, parallel curving ridges that are very similar in morphology to terrestrial scroll bars created during fluvial processes (e.g., Fig. 12a).

Meandering streams with high sinuosity require an extended flow regime while the superposed fans generally form by multiple, shorter events of high-volume flow. A better understanding of the inverted sinuous ridges and associated landforms within the lower member of MFF could provide new information about the history of aqueous processes on this portion of Mars. The variation of thickness of SRs is heavily influenced by the amount of infilling, cementation, and erosion that occurred during the channel's history, and provides at best an estimate for the apparent thickness of the original channel, since the resistant top surface may have protected both channel and non-channel materials from erosion. The long sinuous ridge that extends hundreds of kilometers along a topographic basin of the northern plains materials (Fig. 13), following the low point of a broad basin between lobes of lower member MFF materials, may require additional investigation regarding a possible esker origin for this feature, or perhaps it is simply indicative of sufficient prolonged fluvial input to support flow in this one channel over a great distance. While none of our observations of sinuous ridges provides unequivocal evidence that channel flow is the only viable explanation, the combined characteristics of all SRs observed in HiRISE images from the study area is much more consistent with channel flow, in our opinion, than with any other proposed mechanism of origin for these features.

The preferential occurrence of SRs in the lower member of MFF (Burr et al., 2009) does not place a strong constraint on the emplacement of MFF itself, but it does suggest that lower member MFF emplacement was contemporaneous with some form of fluid flow across the earliest portions of the lower member. Some researchers favor a late Hesperian age for the earliest portions of MFF (Schultz and Lutz, 1988; Schultz, 2007), so that perhaps the fluid flow associated with SR emplacement might actually correlate with the waning stages of extensive fluvial outflow documented across Mars during the Hesperian (Carr, 1996).

6. Future work

The results presented here illustrate the potential for advancing our understanding of aeolian erosion on Mars, but more comprehensive surveys (both in terms of the number of HiRISE images examined and in the total areal extent of MFF materials studied) are needed to achieve a definitive final result. Our initial results suggest that in future studies of yardangs on Mars, the following parameters should be helpful for distinguishing between different groups of yardangs: (1) Length-to-width ratio (potentially related to erosion susceptibility or duration of abrasion). (2) Horizontal dimensions in plan view (the size of yardangs provides a relative indicator of the amount of erosion that has occurred). (3) Height (yardang height can constrain the volume of material removed by erosion). (4) Abrasion slopes (over time, yardangs should have their faces approach specific angles to the wind, similar to relationships observed or predicted for ventifacts, e.g., Sharp, 1948; Bridges et al., 2005). (5) Preservation and characteristics of internal layers (an indication of heterogeneity of the bedrock material, with the stronger materials preserved as more resistant layers within the sediment package). (6) Evidence of erosional notches near the base of yardangs, which may be related to the height at which peak saltation energy was imparted during erosion of the yardang materials (e.g., Section 8.7.4 of McEwen et al., 2007a). No one measurement will likely prove to be diagnostic of a particular type of erosional environment or bedrock type, but consideration of the entire suite of possible measurements (likely including other measurable parameters not considered here) should facilitate discrimination of similarities or differences between yardang locales. Given the comparison above between the lower member yardangs and a single middle member yardang, it would be particularly helpful to carry out surveys of yardangs in both the middle and upper members of MFF. Similarly, for future studies of sinuous ridges, a survey to look for the abundance (or lack) of sinuous ridges in the middle and upper member of MFF would go a long way toward confirming that there is a temporal correlation between sinuous channel formation and the early phases of MFF emplacement.

7. Conclusions

- HiRISE images including exposures of the lower member of the Medusae Fossae Formation (MFF) were used to identify the characteristics of two specific landforms that are well expressed in this particular geologic unit; yardangs and sinuous ridges.

- Yardangs are very abundant in the lower member of MFF, where many individual yardangs show evidence of a caprock unit overlying a more friable unit; layered sequences of resistant-friable components suggest that dozens of such depositional events were part of the emplacement of the lower member of MFF, most likely as multiple ignimbrite deposits.
- Heights of yardangs in the lower member materials are generally less than a few tens of meters. The 35-m height of one yardang (Fig. 2) indicates at least 19,000 km^3 of lower member MFF materials were removed by the erosive action of the wind.
- Sinuous ridges are very common within exposures of the lower member of MFF. Multiple ridge types are present, but all forms are most consistent with some form of aqueous channel flow rather than other possible fluvial origins.

Acknowledgments

The comments of two anonymous reviewers were very helpful in improving an early version of this manuscript. This work was supported in part by NASA Planetary Geology and Geophysics program Grant NNX07AP42G to J.R.Z., and the Planetary Geology and Geophysics Undergraduate Research Program of NASA for L.J.G. to spend the summer of 2008 working at NASM.

References

Baker, V.R., Strom, R.G., Croft, S.K., Gulick, V.C., Kargel, J.S., Komatsu, G., 1991. Ancient oceans, ice sheets and the hydrological cycle on Mars. Nature 352, 589–594.

Bibring, J.-P., and 47 colleagues, 2006. Global mineralogical and aqueous Mars history derived from OMEGA/Mars Express data. Science 312 (5772), 400–404. doi:10.1126/science.1122659.

Bosworth, T., 1922. Geology of the Tertiary and Quaternary Periods in the Northwest Part of Peru. Macmillan, London. pp. 269–309.

Bradley, B.A., Sakimoto, S.E.H., Frey, H., Zimbelman, J.R., 2002. Medusae Fossae Formation: New perspectives from Mars Global Surveyor. J. Geophys. Res. 107 (E8). doi:10.1029/2001JE001537.

Breed, C.S., McCauley, J.F., Whitney, M.I., 1989. Wind erosion forms. In: Thomas, D.S.G. (Ed.), Arid Zone Geomorphology. Belhaven Press, London, pp. 284–307.

Bridges, N.T., Greeley, R., Haldemann, A.F.C., Herkenhoff, K.E., Kraft, M., Parker, T.J., Ward, A.W., 1999. Ventifacts at the pathfinder landing site. J. Geophys. Res. 104, 8595–8615.

Bridges, N.T., Phoreman, J., White, B.R., Greeley, R., Eddlemon, E., Wilson, G., Meyer, 2005. Trajectories and energy transfer of saltating particles onto rock surfaces: Application to abrasion and ventifact formation on Earth and Mars. J. Geophys. Res. 110, 1–24.

Bridges, N.T., Geissler, P.E., McEwen, A.S., Thomson, B.J., Chuang, F.C., Herkenhoff, K.E., Keszthelyi, L.P., Martinez-Alonso, S., 2007. Windy Mars: A dynamic planet as seen by the HiRISE camera. Geophys. Res. Lett. 34, L23205. doi:10.1029/2007GL0231445.

Burr, D.M., Williams, R.M.E., Nussbaumer, J., Zimbelman, J.R., 2006. Multiple, distinct, (glacio?) fluvial paleochannels throughout the western Medusae Fossae Formation, Mars. Lunar and Planetary Science, vol. XXXVII. Lunar and Planetary Institute, Houston (abstract #1367).

Burr, D.M., Enga, M.T., Williams, R.M.E., Zimbelman, J.R., Howard, A.D., Brennand, T.A., 2009. Pervasive aqueous paleoflow features in the Aeolis Mensae/Western Medusae Fossae Formation, Mars. Icarus 200, 52–76. doi:10.1016/j.icarus.2008.10.014.

Byrne, S., Murray, B., 2002. North polar stratigraphy and the paleo-era of Mars. J. Geophys. Res. 107 (E6). doi:10.1029/2001JE001615.

Carr, M.H., 1981. The Surface of Mars. Yale University Press, New Haven, CT.

Carr, M.H., 1996. Water on Mars. Oxford University Press, New York, NY.

Carter, L.M., Campbell, B.A., Watters, T.R., Phillips, R.J., Putzig, N.E., Safaeinili, A., Plaut, J.J., Okubo, C.H., Egan, A.F., Seu, R., Biccari, D., Orosei, R., 2009. Shallow radar (SHARAD) sounding observations of the Medusae Fossae Formation, Mars. Icarus 199, 295–302. doi:10.1016/j.icarus.2008.10.007.

Chapman, M.G., Masursky, H., Dial, A.L., 1989. Geologic maps of science study site 1A, east Mangala Valles, Mars. U.S. Geol. Survey Misc. Invest. Series Map I-1962, scale 1:500,000.

Christensen, P.R., 1986. Regional dust deposits on Mars: Physical properties, age, and history. J. Geophys. Res. 91, 3533–3545.

Christensen, P.R., and 12 colleagues, 2001. Mars global surveyor thermal emission spectrometer experiment: Investigation description and surface science results. J. Geophys. Res. 106 (10), 23823–23871.

Christensen, P.R., and 10 colleagues, 2004. The Thermal Emission Imaging System (THEMIS) for the Mars 2001 Odyssey mission. Space Sci. Rev. 110, 85–110.

Edgett, K.S., 2005. The sedimentary rocks of Sinus Meridiani: Five key observations from data acquired by the Mars Global Surveyor and Mars Odyssey orbiters. Mars J. 1, 5–58.

Edgett, K.S., Williams, R.M.E., Malin, M.C., Cantor, B.A., Thomas, P.C., 2003. Mars landscape evolution: Influence of stratigraphy on geomorphology in the north polar region. Geomorphology 52, 289–297. doi:10.1016/S0269-555X(02)00262-3.

Ehlmann, B.L., and 13 colleagues, 2008. Orbital identification of carbonate-bearing rocks on Mars. Science 322, 1828–1832. doi:10.1126/science.1164759.

Fishbaugh, K.E., Head, J.W., 2005. Origin and characteristics of the Mars north polar basal unit and implications for polar geologic history. Icarus 174, 444–474. doi:10.1016/j.icarus.2004.06.021.

Forsythe, R.D., Zimbelman, J.R., 1988. Is the Gordii Dorsum escarpment an exhumed transcurrent fault? Nature 336, 143–146.

Forsythe, R.D., Zimbelman, J.R., Barlow, N.G., 1991. Comparison of data sets (topographic, geology, geophysics, cratering) for Mars' western equatorial transition zone. Lunar and Planetary Science, vol. XXII. Lunar and Planetary Institute, Houston. pp. 403–404.

Glotch, T.D., Rogers, A.D., 2009. Reexamination of global carbonate abundances using TES data. Lunar and Planetary Science, vol. XL. Lunar and Planetary Institute, Houston (abstract #1605).

Greeley, R., Iversen, J.D., 1985. Wind as a Geological Process. Cambridge University Press, Cambridge, MA.

Greeley, R., Guest, J.E., 1987. Geologic map of the eastern equatorial region of Mars. U.S. Geol. Survey Misc. Invest. Series Map I-1802-B, scale 1:15,000,000.

Griffin, L.J., Zimbelman, J.R., 2009. Geologic mapping of western Medusae Fossae Formation, Mars (MC 23-NW): Redefining unit boundaries and features to reveal a history of tectonism, wind erosion, and episodic water flow. Lunar and Planetary Science, vol. XL. Lunar and Planetary Institute, Houston (abstract 1196).

Halimov, M., Fezer, F., 1989. Eight yardang types in central Asia. Zeits. Geomorph. 33, 205–217.

Hobbs, W.H., 1917. The erosional and degradational processes of deserts, with especial reference to the origin of desert depressions. Ann. Assoc. Am. Geogr. 7, 25–60.

Howard, A.D., 1981. Etched plains and braided ridges of the south polar region of Mars: Features produced by basal melting of ground ice? Reports of the Planetary Geology Program, NASA TM 84211, 286–288.

Hynek, B.M., Phillips, R.J., Arvidson, R.E., 2003. Explosive volcanism in the Tharsis region: Global evidence in the Martian geologic record. J. Geophys. Res. 108 (E9). doi:10.1029/2003JE002062.

Kargel, J.S., Strom, R.G., 1992. Ancient glaciation on Mars. Geology 20, 3–7.

Kerber, L., Head, J.W., 2009. The age of the Medusae Fossae Formation: Reassessment using lava flow cast and mold contacts. Lunar and Planetary Science, vol. XL. Lunar and Planetary Institute, Houston (abstract #2235).

Kieffer, H.H., Martin, T.Z., Peterfreund, A.R., Jakosky, B.M., Miner, E.D., Palluconi, F.D., 1977. Thermal and albedo mapping of Mars during the Viking primary mission. J. Geophys. Res. 82, 4249–4291.

Mainguet, M., 1968. Le Bourkou – Aspects d'un modelé éolien. Ann. Geogr. 77, 296–322.

Mainguet, M., 1972. Le Modelé des Grès. Institut Geographique National, Paris. 657 p.

Malin, M.C., 1979. Evidence of indurated deposits of fine materials. NASA Conf. Pub. 2072 (abstract), p. 54.

Malin, M.C., Edgett, K.S., 2001. Mars Global Surveyor Mars Orbiter Camera: Interplanetary cruise through primary mission. J. Geophys. Res. 106, 23429–23570.

Malin, M.C., Edgett, K.S., 2003. Evidence for persistent flow and aqueous sedimentation on early Mars. Science 302, 1931–1934. doi:10.1126/science.1090544.

Malin, M.C., and 17 colleagues, 1998. Early views of the martian surface from the Mars Orbiter Camera of Mars Global Surveyor. Science 279, 1681–1685.

Malin, M.C., and 13 colleagues, 2007. Context Camera investigation on board the Mars Reconnaissance Orbiter. J. Geophys. Res. 112, E05S04. doi:10.1029/2006JE002808.

Mangold, N., Quantin, C., Ansan, V., Delacourt, C., Allemand, P., 2004. Evidence for precipitation on Mars from dendritic valleys in the Valles Marineris area. Science 305, 78–81.

Mandt, K.E., de Silva, S.L., Zimbelman, J.R., Crown, D.A., 2008. The origin of the Medusae Fossae Formation, Mars: Insights from a synoptic approach. J. Geophys. Res. – Planets 113, E12011. doi:10.1029/2008JE003076.

Mann, A.W., Horowitz, R.C., 1979. Groundwater calcrete deposits in Australia: Some observations from Western Australia. J. Geol. Soc. Aust. 26, 293–303.

McCauley, J.F., 1973. Mariner 9 evidence for wind erosion in the equatorial and mid-latitude regions of Mars. J. Geophys. Res. 78, 717–751.

McCauley, J.F., Breed, C.S., Grolier, M.J., 1977. Yardangs. In: Doehring, D.O. (Ed.), Geomorphology in Arid Regions. Allen & Unwin, Boston, pp. 33–269.

McEwen, A.S., and 14 colleagues, 2007a. Mars Reconnaissance Orbiter's High Resolution Imaging Science Experiment (HiRISE). J. Geophys. Res. 112, E05S02. doi:10.1029/2005JE002605.

McEwen, A.S., and 32 colleagues, 2007b. A closer look at water-related geologic activity on Mars. Science 317, 1706–1709. doi:10.1126/science.1143987.

McMenamin, D.S., McGill, G.E., 2005. Processes involved in the formation of martian fan-shaped deposits. Lunar and Planetary Science, vol. XXXVI. Lunar and Planetary Institute, Houston (abstract #1732).

Moore, J.M., Howard, A.D., Dietrich, W.E., Schenk, P.M., 2003. Martian layered fluvial deposits: Implications for Noachian climate scenarios. Geophys. Res. Lett. 24. doi:10.1029/2003GL019002.
Mouginis-Mark, P.J., 1993. The influence of oceans on martian volcanism. Lunar and Planetary Science, vol. XXIV. Lunar and Planetary Institute, Houston. pp. 1021–1022.
Murchie, S., and 49 colleagues, 2007. Compact Reconnaissance Imaging Spectrometer for Mars (CRISM) on Mars Reconnaissance Orbiter (MRO). J. Geophys. Res. 112, E05S03. doi:10.1029/2006JE002682.
Nimmo, F., Tanaka, K., 2005. Early crustal evolution of Mars. Ann. Rev. Earth Planet. Sci. 33, 133–161. doi:10.1146/annurev.earth.33.092203.122637.
Nussbaumer, J., 2007. Possible sea sediments due to glaciofluvial activity in Elysium Planitia, Mars. Seventh International Conference on Mars. Lunar and Planetary Institute, Houston, TX (abstract #1353).
Pain, C.F., Oilier, C.D., 1995. Inversion of relief: A component of landscape evolution. Geomorphology 12 (2), 151–165.
Pain, C.P., Clarke, J.D.A., Thomas, M., 2007. Inversion of relief on Mars. Icarus 190, 478–491.
Palluconi, F.D., Kieffer, H.H., 1981. Thermal inertia mapping of Mars from 60°S to 60°N. Icarus 45 (2), 415–426.
Parker, T.J., 1991. A comparison of the martian Medusae Fossae Formation with terrestrial carbonate platforms. Lunar and Planetary Science, vol. XXII. Lunar and Planetary Institute, Houston. pp. 1029–1030.
Parker, T.J., Saunders, R.S., Schneeberger, D.M., 1989. Transitional morphology in the west Deuteronilus Mensae region of Mars: Implications for modification of the lowland/upland boundary. Icarus 82, 111–145.
Press, F., Siever, R., 1974. Earth. W.H. Freeman and Co., San Francisco.
Pruis, M.J., Tanaka, K.L., 1995. The martian northern plains did not result from plate tectonics. Lunar and Planetary Science, vol. XXVI. Lunar and Planetary Institute, Houston. pp. 1147–1148.
Sakimoto, S.E.H., Frey, H.V., Garvin, J.B., Roark, J.H., 1999. Topography, roughness, layering, and slope properties of the Medusae Fossae Formation from Mars Orbiter Laser Altimeter (MOLA) and Mars Orbiter Camera (MOC) data. J. Geophys. Res. 104 (E10), 24141–24154.
Schultz, P.H., 2007. Planetary science: Hidden Mars. Science 318 (5853), 1080–1081. doi:10.1126/science.1151412.
Schultz, P.H., Lutz, A.B., 1988. Polar wandering on Mars. Icarus 73, 91–141.
Scott, D.H., Tanaka, K.L., 1982. Ignimbrites of Amazonis Planitia region of Mars. J. Geophys. Res. 87, 1179–1190.
Scott, D.H., Tanaka, K.L., 1986. Geologic map of the western equatorial region of Mars. U.S. Geol. Survey Misc. Invest. Series Map I-1802-A, scale 1:15,000,000.
Sharp, R.P., 1948. Pleistocene ventifacts east of the Big Horn Mountains, Wyoming. J. Geol. 57, 173–195.
Shockey, K.M., Zimbelman, J.R., 2005. The Medusae Fossae Formation: Mapping the origins. Lunar and Planetary Science, vol. XXVI. Lunar and Planetary Institute, Houston (abstract #1799).
Sleep, N.H., 1994. Martian plate tectonics. J. Geophys. Res. 99, 5639–5655.
Smith, D.E., and 18 colleagues, 1998. Topography of the northern hemisphere of Mars from the Mars Orbiter Laser Altimeter. Science 279, 1686–1692.
Tanaka, K.L., 1986. The stratigraphy of Mars. J. Geophys. Res. 91, 139–158.
Tanaka, K.L., 2000. Dust and ice deposition in the martian geologic record. Icarus 144 (2), 254–266. doi:10.1006/icar.1999.6297.
Walker, A.S., 1986. Chapter 8: Eolian. In: Short, N.M., Blair, R.W., (Eds), Geomorphology from space, NASA SP (geoinfo.amu.edu.pl/wpk/geos/GEO_HOME_PAGE.html).
Ward, A.W., 1979. Yardangs on Mars: Evidence of recent wind erosion. J. Geophys. Res. 84, 8147–8166.
Ward, A.W., Greeley, R., 1984. Evolution of the yardangs at Rogers Lake, California. Geol. Soc. Am. Bull. 95, 829–837.
Watters, T.R., Campbell, B., Carter, L., Leuschen, C.J., Plaut, J.J., Picardi, G., Orosei, R., Safaeinili, A., Clifford, S.M., Farrell, W.M., Ivanov, A.B., Phillips, R.J., Stofan, E.R., 2007. Radar sounding of the Medusae Fossae Formation Mars: Equatorial ice or dry, low-density deposits? Science 318, 1125–1128.
Wells, G.L., Zimbelman, J.R., 1997. Extraterrestrial arid surface processes. In: Thomas, D.S.G. (Ed.), 2nd ed., Arid Zone Geomorphology: Process, Form and Change in Drylands John Wiley & Sons, New York, NY, pp. 659–690.
Werner, S.C., 2006. Major aspects of the chronostratigraphy and geologic evolutionary history of Mars. Ph.D. dissertation, Freie University, Berlin, 165 p. (www.diss.fu-berlin.de/2006/33/indexe.html).
Whitney, M.I., 1983. Eolian features shaped by aerodynamic and vorticity processes. In: Brookfield, M.E., Ahlbrandt, T.S. (Eds.), Eolian Sediments and Processes. Elsevier, Amsterdam, pp. 23–245.
Whitney, M.I., 1985. Yardangs. J. Geol. Ed. 33, 93–96.
Williams, R.M.E., 2007. Global spatial distribution of raised curvilinear features on Mars. Lunar Planet Science, vol. XXXVIII. Lunar and Planetary Institute, Houston (abstract #1821).
Williams, R.M.E., 2008. Inverted paleochannels on Earth and Mars. www.psi.edu/pgwg/images/may08image.html.
Williams, R.M.E., Edgett, K.S., 2005. Valleys in the martian rock record. Lunar and Planetary Science, vol. XXXVI. Lunar and Planetary Institute, Houston (abstract #1099).
Williams, R.M.E., Malin, M.C., Edgett, K.S., 2005. Remnants of the courses of fine-scale, precipitation-fed runoff streams preserved in the martian rock record. Lunar and Planetary Science, vol. XXXVI. Lunar and Planetary Institute, Houston (abstract #1173).
Williams, R.M.E., Chidsey Jr., T.C., Eby, D.E., 2007. Exhumed paleochannels in central Utah: Analogs for raised curvilinear features on Mars. In: Willis, G.C., Hylland, M.D., Clark, D.L., Chidsey, T.C. (Eds.), Central Utah: Diverse geology of a dynamic landscape, Utah Geological Association Pub. 36, Salt Lake City, Utah.
Williams, R.M.E., Irwin, R.P., Zimbelman, J.R., 2009. Evaluation of paleohydrologic models for inverted channels: Applications to Mars. Geomorphology. doi:10.1016/j.geomorph.2008.12.01.
Zimbelman, J.R., 1995. An examination of hypotheses of formation for the enigmatic massive deposits in Amazonis Planitia, Mars. Lunar and Planetary Science, vol. XXVI. Lunar and Planetary Institute, Houston. pp. 1559–1560.
Zimbelman, J.R., 2008. Geologic mapping of the MC-23 NW quadrangle on Mars. Zimbelman_final.pdf. U.S. Geol. Surv. Open File Report, 2008 Planetary Geologic Mapping meeting, Flagstaff, AZ.
Zimbelman, J., Crown, D., Grant, J., Hooper, D., 1997. The Medusae Fossae Formation, Amazonis Planitia, Mars: Evaluation of proposed hypotheses of origin. Lunar and Planetary Science, vol. XXVIII. Lunar and Planetary Institute, Houston. pp. 1559–1560.
Zimbelman, J., Hooper, D., Crown, D., Grant, J., Sakimoto, S., Frey, H., 1999. Medusae Fossae Formation, Mars: An assessment of possible origins utilizing early results from Mars Global Surveyor. Lunar and Planetary Science, vol. XXX. Lunar and Planetary Institute, Houston (abstract #1652).
Zimbelman, J.R., Sakimoto, S.E.H., Frey, H., 2000. Evidence for a fluvial contribution to the complex story of the Medusae Fossae Formation on Mars. Geol. Soc. Am. Abs. Prog. 32 (7), A303.